Development of second-order gradient DC SQUIDs for the readout of superconducting TES detectors

Z.F. Feng[a,b], X.F. Zhou[a,b], Q.X. Ma[a,b], W. Zhang[*a], P.Z. Li[a], Z. Wang[a], J.Q. Zhong[a], W. Miao[a], Y. Ren[a], Q.J. Yao[a], V. Koshelets[c], L. Filippenko[c], M. Fominsky[c], J. Li[a], and S.C. Shi[a]

[a]Purple Mountain Observatory, CAS, Nanjing, 210023, China

[b]University of Science and Technology of China, Hefei, 230026, China

[c]Kotel'nikov Institute of Radio Engineering and Electronics, Russian Academy of Sciences, Russia

*wzhang@pmo.ac.cn

ABSTRACT

Superconducting transition-edge sensors (TESs) are highly sensitive detectors, can detect electromagnetic wave radiations from millimeter/submillimeter, optical to x/γ rays, suitable for astrophysics, quantum information, and biosensing. Direct current superconducting quantum interference devices (DC SQUIDs) are the detector of choice for TES readout, thanks to their low noise, low impedance, and low power dissipation. In this work, we designed the DC SQUID with a second-order gradient structure, which can effectively mitigate the effect of external magnetic flux. We optimized the fabrication process and successfully fabricated the high-performance DC SQUID with Nb/Al-AlOx/Nb Josephson junctions (critical current density: $J_C \sim 1 \mu A/\mu m^2$). The properties of the fabricated DC SQUID were in good agreement with the simulation results. Meanwhile, the measured flux noise was 6 $\mu\Phi_0/\sqrt{\text{Hz}}$, corresponding to a current noise of 100 $\text{pA}/\sqrt{\text{Hz}}$. Furthermore, we demonstrated the capability of the DC SQUID to read out the TES detector, including I-V curves, photon pulse response, and noise performance.

Keywords: DC SQUID, Josephson junction, flux noise, TES

1. INTRODUCTION

The superconducting transition-edge sensors (TESs) can be used as a bolometer for power measurement and a calorimeter for energy-resolved single-photon detection [1]. Voltage-biased within the sharp resistive transition region [2], TESs show high sensitivity and have been used in large scientific instruments for astronomy [3], quantum information [4], and particle physics [5]. However, in the early stage of TES development, it was found difficult to match the traditional FET amplifiers to low-impedance TESs. Superconducting quantum interference devices (SQUIDs) with quantum-limited noise and ultralow power dissipation are easily matched to TES devices [6]. For the readout of a single TES device, a two-stage SQUID readout scheme is typically employed [7]. The first stage with a single DC SQUID is low noise, and its current output modulates a series array of non-hysteric SQUIDs in the second stage via a common modulation line [8]. The second stage is designed to have high gain such that the output signal exceeds the noise of the room-temperature electronics. In this way, two-stage SQUIDs preserve low noise, large dynamic range, and high bandwidth.

Meanwhile, a large TES array can improve the collection area, counting rate, and sensitivity. Consequently, multiplexing readout technologies [9,10] combine the signals of tens to thousands of TESs into a single readout line, reducing the complexity of wiring, thermal load, and cost. Multiplexing schemes such as time-division multiplexing (TDM), code-division multiplexing (CDM), frequency-division multiplexing (FDM), and microwave SQUID multiplexing (μMUX) require SQUIDs to amplify the TES signal. Consequently, the noise performance of multiplexers is determined by SQUIDs.

Infrared, Millimeter-Wave, and Terahertz Technologies XII, edited by Cunlin Zhang, Xi-Cheng Zhang, Masahiko Tani, Proc. of SPIE Vol. 13726, 1372609 · 2025 Published by SPIE
0277-786X · doi: 10.1117/12.3073803

The SQUID is highly susceptible to external flux, and a gradient configuration can reduce the flux pickup of ambient magnetic fields [11]. A second-order gradiometer typically consists of four parallel lobes, whose orientation alternates around the SQUID, making the SQUID insensitive to both first-order gradients and uniform fields.

We are developing the μMUX based on an Nb-based resonator and second-order gradient RF SQUID [12]. In this study, we further design and fabricate a single-stage DC SQUID for the readout of TES detectors. Its properties, including current-voltage characteristics, voltage-flux response, flux noise, and current noise, are thoroughly measured. This DC SQUID was finally used to read out the TES detector characteristics.

2. DESIGN AND FABRICATION

2.1 DC SQUID Design

We designed the DC SQUID with a cross-coupling structure like that in Ref. [13-15]. As shown in Figure 1, DC SQUID loop is a second-order gradient structure consisting of four parallel lobes arranged like a cloverleaf. Each lobe is an octagonal slotted washer with the input coil and feedback coil running in the slot. The feedback and input coils are 0.5 and 1.5 turns around each lobe, respectively. The self and mutual inductances between the coils and the SQUID loop are calculated using COMSOL software. The SQUID loop is interrupted by two Josephson junctions (JJs) with a junction diameter (D) of 3.4 μm. With the measured critical current density of $J_C \approx 0.75$ μA/μm^2 from previously fabricated batches, the critical current I_C of the JJ is 7 μA at a bath temperature of 4.2 K. Each junction is resistively shunted by two resistors with $R_{sh} = 2.7$ Ω to suppress hysteretic behavior. The shunt resistors are thermally anchored to the cooling fins to mitigate hot-electron effects [16]. Taking the specific capacitance $C_S = 40.3$ fF/μm^2 into account, the hysteresis parameter $\beta_C = 2\pi I_C R_{sh}^2 C_J/\Phi_0$ is 0.06, where C_J denotes JJ capacitance ($C_J = C_S \times S$), $S = \pi(D/2)^2$ is the junction area, Φ_0 the magnetic flux quantum. Screening parameter is $\beta_L = 2I_c L_S/\Phi_0 \sim 0.34$, where L_S denotes the loop self-inductance of the DC SQUID. The key simulation and design parameters of the DC SQUID are summarized in Table 1.

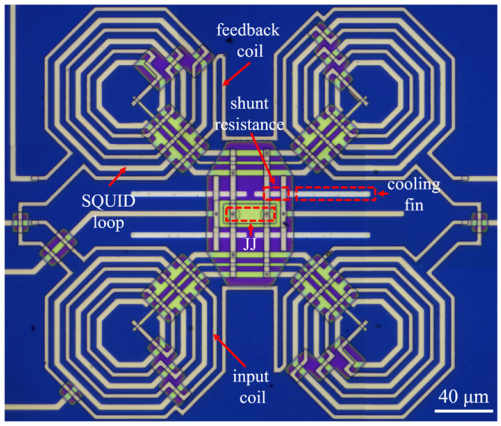

Figure 1. An optical microscope image of the DC SQUID

Table 1 Simulation and design parameters of the DC SQUID

Parameter	L_S [pH]	M_{in} [pH]	M_{fb} [pH]	J_C [μA/μm^2]	S [μm^2]	I_C [μA]	β_C	β_L
Value	51.4	146.7	29.4	0.75	9	7	0.06	0.34

2.2 DC SQUID Fabrication

The DC SQUID was fabricated based on the fabrication process of high-quality Nb/Al-AlOx/Nb JJs. Figure 2 shows the schematic of the main layers of DC SQUID chips. High-resistivity silicon substrate is covered by a 100-nm thick Al_2O_3 layer as a stop layer for the following etching process. Firstly, a 150-nm Nb layer, deposited with magnetron sputtering,

was etched using the reactive ion etching (RIE) technique to form the DC SQUID loop. Then, the Nb/Al-AlOx/Nb trilayer structure was formed and patterned on the central region of the DC SQUID loop. The Nb bottom and top electrode were 100 and 70 nm in thickness, respectively. The Al film was oxidized in a pure O_2 atmosphere to form the Al-AlOx barrier layer. The size of JJs is defined by etching the Nb top electrode. Note that the Al-AlOx barrier was slightly larger than that of the JJ to avoid uncontrollable lateral corrosion. To provide electrical insulation between two superconducting layers, a 250-nm thick SiO_2 layer was deposited and patterned by a lift-off technique. A 70-nm thick Mo layer was deposited to form the shunt resistor. Finally, a 350-nm Nb wiring connects the JJ to the SQUID loop and provides connections to the input and feedback coils, etc.

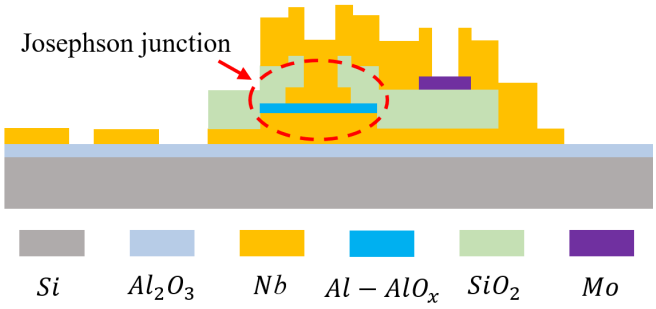

Figure 2. Schematic of the main layers of DC SQUID chip.

3. MEASUREMENT SETUP AND RESULTS

3.1 Measurement setup

We measured the performance of DC SQUID and TES in a dilution refrigerator (Triton 400, Oxford Instruments) with a base temperature below 20 mK. The TES detector was anchored to a copper holder and then mounted on the mixing chamber stage (~20 mK) [17]. As shown in Figure 3, the TES detector is voltage-biased via a 0.33 Ω bias resistor R_b. The DC SQUID surrounded by an Nb shield was mounted on the 3.5-K plate. A low-noise, high-bandwidth room-temperature electronics (XXF-1) from Magnicon GmbH [18] was used to characterize the DC SQUID. To measure the optical response of the TES detector, a 1550-nm pulsed laser was attenuated via an optical attenuator, then coupled to the TES detector. The output signal of the TES detector was recorded using a digital oscilloscope.

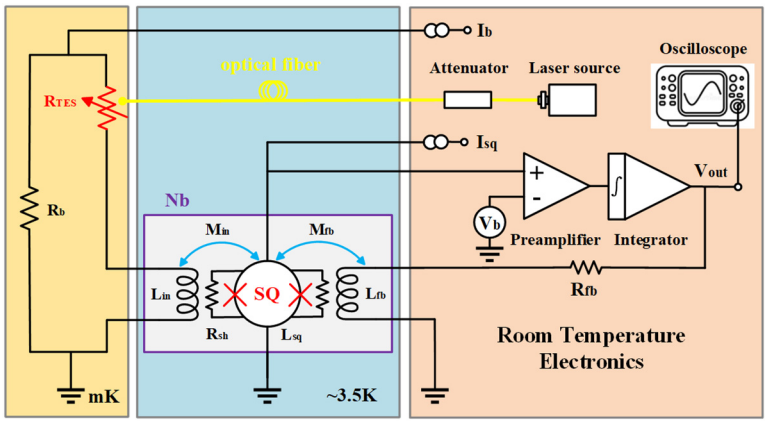

Figure 3. Measurement diagram of DC SQUID and TES detector.

3.2 DC SQUID results

The current-voltage (I-V) curves of the fabricated DC SQUID are shown in Figure 4(a) for external magnetic fluxes $\Phi = n\Phi_0$ and $\Phi = (n \pm 1/2)\Phi_0$. The critical current of the DC SQUID is $I_C \approx 2I_{C0}\cos(\pi\Phi/\Phi_0)$. Here, the intrinsic critical current I_{C0} of single junction is estimated to 7.3 μA. Some small distortions appear, related to the fundamental SQUID resonance [19]. Figure 4(b) presents the voltage-flux (V-Φ) modulation curves of the feedback coil under different SQUID bias currents I_{sq}. The feedback coil current, sweeping from −125 μA to 125 μA, corresponds to approximately 3.5

modulation periods. Thus, the current sensitivity of the feedback coil $1/M_{fb}$ is 71.3 μA/Φ_0, and the mutual inductance between the SQUID loop and the feedback coil is $M_{fb} = 29$ pH. Similarly, V-Φ measurement through the input coil gives the current sensitivity $1/M_{in} \approx 14.7$ μA/Φ_0 and the mutual inductance between the SQUID loop and the input coil $M_{in} \approx$ 140.6 pH. These results agree with the simulation results in Table 1.

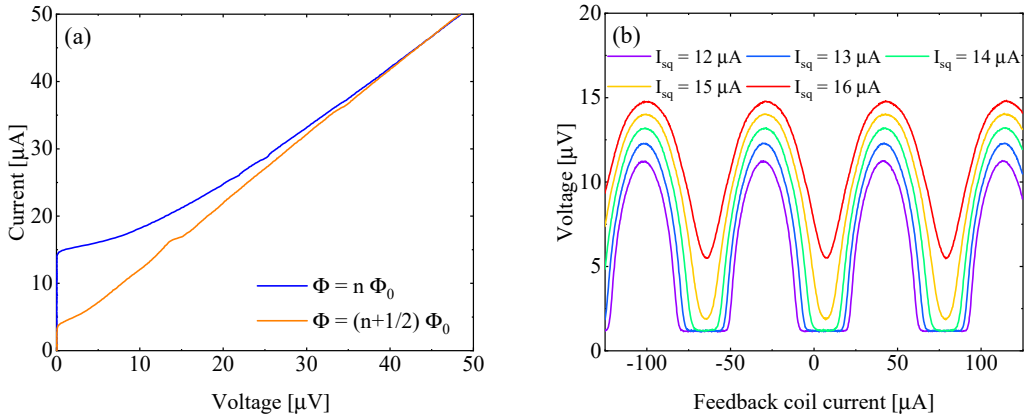

Figure 4. (a) Current-voltage curves and (b) voltage-flux curves of the DC SQUID at 3.5 K.

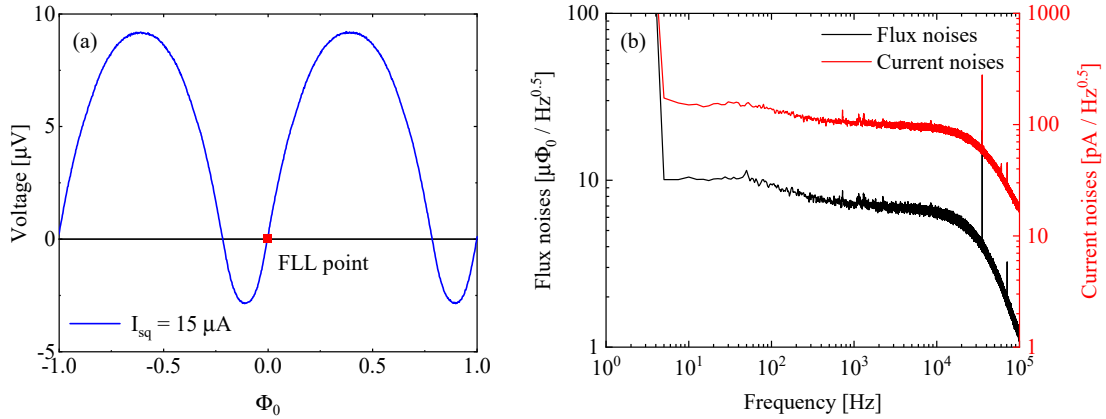

Figure 5. (a) Voltage-flux curve of FLL point. (b) The measured flux and current noise spectra of DC SQUID.

Figure 5(a) shows the V-Φ curve of the DC SQUID at $I_{sq} = 15$ μA. The voltage swing V_{pp} is 12 μV, and the flux-to-voltage transfer coefficient is $V_\Phi \approx 51.6$ μV/Φ_0 at the steepest working point, where the DC SQUID was flux-locked. Figure 5(b) shows the measured flux and current noise spectra. The flux white noise $\sqrt{S_\Phi} = \sqrt{S_V} \times (M_{fb}/R_f)$ is about 6.5 μ$\Phi_0/\sqrt{\text{Hz}}$@10 kHz, where $\sqrt{S_V}$ represents the measured voltage noise and R_f denotes the feedback resistance. $\sqrt{S_\Phi}$ is mainly determined by the SQUID intrinsic noise $\sqrt{S_{\Phi,int}}$, and the voltage noise $\sqrt{S_{V,electronics}}$ and current noise $\sqrt{S_{I,electronics}}$ of the room-temperature readout electronics [20]

$$\sqrt{S_\Phi} = \sqrt{S_{\Phi,int} + S_{\Phi,V,electronics} + S_{\Phi,I,electronics}} = \sqrt{S_{\Phi,int} + S_{V,electronics}/V_\Phi^2 + S_{I,electronics}(R_{dyn}/V_\Phi)^2} \quad (1)$$

Here $\sqrt{S_{\Phi,V,electronics}}$ and $\sqrt{S_{\Phi,I,electronics}}$ denote the equivalent flux noise components at the input termination, converted from $\sqrt{S_{V,electronics}}$ and $\sqrt{S_{I,electronics}}$, respectively, and R_{dyn} is the dynamic resistance at the working point. According to the parameters of the DC SQUID and room-temperature electronics, we obtained $\sqrt{S_{\Phi,V,electronics}} \sim 6.4$ μ$\Phi_0/\sqrt{\text{Hz}}$ and $\sqrt{S_{\Phi,I,electronics}} \sim 0.1$ μ$\Phi_0/\sqrt{\text{Hz}}$. However, $\sqrt{S_{\Phi,int}}$ is generally less than 0.5 μ$\Phi_0/\sqrt{\text{Hz}}$ [21, 22]. Therefore, the room-temperature readout electronic noise is the dominant component, and it is necessary to enhance V_Φ to realize a low-noise SQUID readout. There are several ways, such as series SQUID arrays (SSA) [23], an additional positive feedback (APF)

[24], or asymmetrical SQUID [25]. The current noise of the DC SQUID is then obtained as $\sqrt{S_I} = \sqrt{S_\Phi}/M_{in} \approx 100\ \mathrm{pA}/\sqrt{\mathrm{Hz}}$ @10 kHz.

3.3 TES electrical characteristics

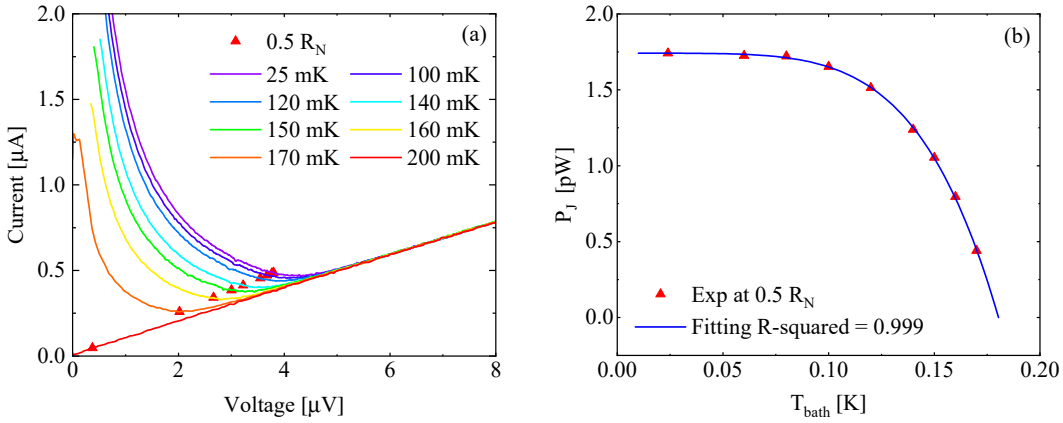

Figure 6. (a) Current-voltage characteristics and (b) Joule power as a function of bath temperature of TES detector

Using this DC SQUID, we further measured I-V curves of a TES detector at different bath temperatures (T_{bath}) from 25 mK to 200 mK (see Figure 6(a)). Joule power ($P_J = I \times V$) at $0.5R_N$ as a function of T_{bath} is plotted in Figure 6(b). The power flow from the electrons to the bath can be described as [1]

$$P_J = K(T_c^n - T_{bath}^n) \tag{2}$$

where T_C is the critical temperature of the TES detector, K and n are constants that depend on the TES detector and the dominant thermal transport mechanism. K, n, and T_C are determined by fitting Equation (2) to the measured P_J vs. T_{bath}. Thermal conductance (G) between the TES detector and the substrate is calculated in terms of the obtained parameters [1]

$$G = nKT_c^{n-1} \tag{3}$$

The fundamental phonon-noise determined noise equivalent power is $NEP_{phonon} = \sqrt{4k_B T_c^2 G} = 1 \times 10^{-17}\ W/\sqrt{Hz}$, where k_B is the Boltzmann constant. These key parameters are listed in Table 2.

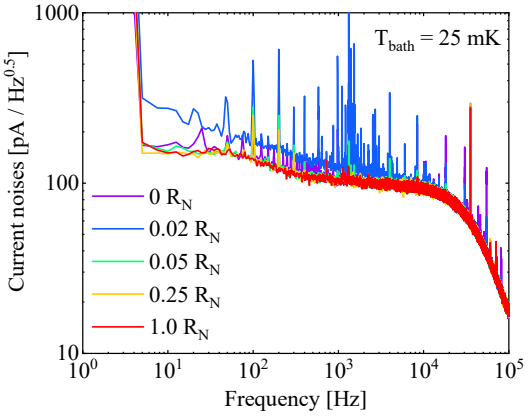

Figure 7. The measured current noise spectra of TES at 25 mK at different working points.

Figure 7 presents the current noise spectra measured across various TES resistances R_{TES} at $T_{bath} = 25\ mK$. The current noise of the TES detector should strongly depend on R_{TES} and is roughly proportional to $1/R_{TES}$ [17]. However, the measured current noise remains nearly constant, $\sqrt{S_I} \approx 100\ \mathrm{pA}/\sqrt{\mathrm{Hz}}$ @10 kHz, independent of R_{TES}, indicating that the noise level is limited by the DC SQUID as well as its readout electronics.

Table 2 The key parameters of the TES detector

Parameter	T_C [mK]	R_N [Ω]	n	G [pW/K]	K	NEP_{phonon} $[10^{-17}\mathrm{W}/\sqrt{\mathrm{Hz}}]$
Value	183	10.4	4.9	50	8.2×10^{-9}	1

3.4 TES optical characteristics

We measured the response of the TES detector at 25 mK with a 1550-nm pulsed laser. As shown in Figure 8(a), the measured pulse response is fitted to a double exponential function [26]

$$V(t) = V_0[\exp(-\frac{t-t_0}{\tau_{el}}) - \exp(-\frac{t-t_0}{\tau_{eff}})] \tag{4}$$

where V_0 and t_0 are constant parameters, τ_{el} and τ_{eff} are electric and effective time constants. The obtained τ_{eff} is 5.8 μs at $0.25R_N$. As shown in Figure 8(b), τ_{eff} is shortest in the intermediate region, where the negative feedback is stronger (loop gain is higher).

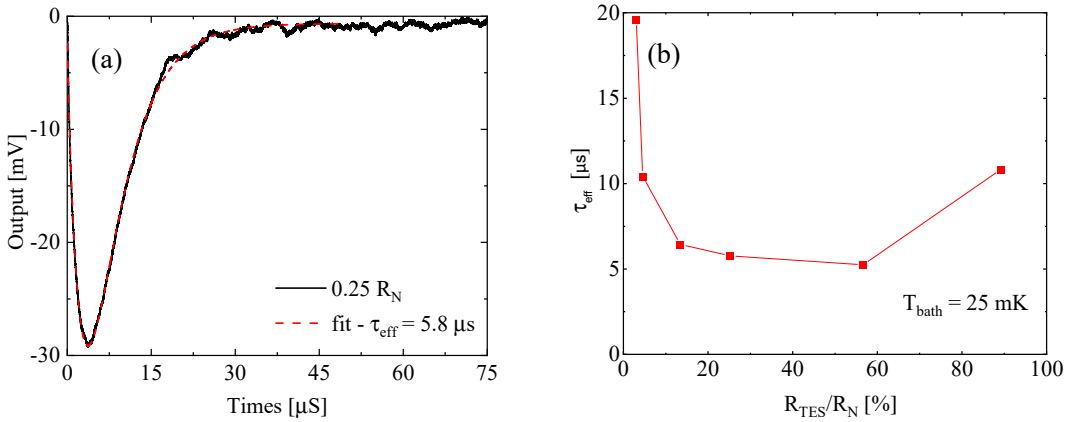

Figure 8. (a) The measured and fitted pulse response (b) The measured effective response time as a function of bias resistance

4. CONCLUSION

In summary, we developed the DC SQUID with a second-order gradient structure, which is in good agreement with the simulation results. The measured flux noise was 6 $\mu\Phi_0/\sqrt{\mathrm{Hz}}$, corresponding to a current noise of 100 $\mathrm{pA}/\sqrt{\mathrm{Hz}}$. This DC SQUID is used to read out the TES detector successfully. We will improve the flux-to-voltage transfer coefficient V_Φ to achieve better noise.

ACKNOWLEDGEMENTS

The authors would like to thank Dr. Wen-Tao Wu of Shanghai Institute of Microsystem and Information Technology for useful discussion on SQUID. This work is supported partly by National Key R&D program of China under Grant 2023YFC2206600, NSFC under Grant 12293032 and 12020101002, and by Ministry of Science and Higher Education of the Russian Federation under Grant 075-15-2024-538.

REFERENCES

[1] Irwin K D, Hilton G C., “Transition-edge sensors,” in Cryogenic Particle Detection. 99:63-150 (2005).
[2] Irwin K D., “An application of electrothermal feedback for high resolution cryogenic particle detection." Appl. Phys. Lett. 66(15): 1998-2000 (1995).

[3] Kuo C L, Bock J J, Bonetti J A, et al., “Antenna-coupled TES bolometer arrays for CMB polarimetry,” Proc. SPIE. 7020: 415-428 (2008).
[4] Lolli L, Brida G, Degiovanni I P, et al., “Ti/Au TES as superconducting detector for quantum technologies,” Int. J. Quantum Inf. 9(supp01): 405-413 (2011).
[5] Li D, Alpert B K, Becker D T, et al., “TES x-ray spectrometer at SLAC LCLS-II,” J Low Temp Phys. 193(5): 1287-1297 (2018).
[6] Irwin K D, Nam S W, Cabrera B, et al., “A self-biasing cryogenic particle detector utilizing electrothermal feedback and a SQUID readout," IEEE Trans. Appl. Supercond. 5(2): 2690-2693 (1995).
[7] Cantor R, Lee L P, Matlashov A, et al., “A low-noise, two-stage DC SQUID amplifier with high bandwidth and dynamic range,” IEEE Trans. Appl. Supercond. 7(2): 3033-3036 (1997).
[8] Welty R P, Martinis J M., “Two-stage integrated SQUID amplifier with series array output,” IEEE Trans. Appl. Supercond. 3(1): 2605-2608 (2002).
[9] Ullom J N, Bennett D A., “Review of superconducting transition-edge sensors for x-ray and gamma-ray spectroscopy,” Supercond. Sci. Technol. 28(8): 084003 (2015).
[10] Wu X, Yu Q, He Y, et al., “Multiplexing technology based on SQUID for readout of superconducting transition-edge sensor arrays,” Chin. Phys. B. 31(10): 108501 (2022).
[11] Clarke J, and Braginski A I, “The SQUID handbook: Vol. I Fundamentals and technology of SQUIDs and SQUID systems,” John Wiley & Sons, (2006).
[12] Feng Z F, Yang X K, Zhang W, et al., “Microwave SQUID multiplexer for readout of transition-edge sensor array,” Proc. SPIE. 12776:233-241 (2023).
[13] Kempf S, Ferring A, Fleischmann A, et al., “Direct-current superconducting quantum interference devices for the readout of metallic magnetic calorimeters,” Supercond. Sci. Technol. 28(4): 045008 (2015).
[14] Xu D, Zhong Q, Cao W H, et al., “A second-order gradiometric superconducting quantum interference device current sensor with cross-coupled structure,” Acta Phys. Sin. 70(12): 128501 (2021).
[15] Xu D, Li J, Wang S, et al., “Low-noise second-order gradient SQUID current sensors overlap-coupled with input coils of different inductances,” Supercond. Sci. Technol. 35(8): 085004 (2022).
[16] Wellstood F C, Urbina C, Clarke J., “Hot-electron effects in metals,” Phys. Rev. B. 49(9): 5942 (1994).
[17] Zhang W, Geng Y, Wang Z, et al., “Development of titanium-based transition-edge single-photon detector,” IEEE Trans. Appl. Supercond. 29(5): 1-5 (2019).
[18] Drung D, Hinnrichs C, Barthelmess H J., “Low-noise ultra-high-speed dc SQUID readout electronics,” Supercond. Sci. Technol. 19(5): S235 (2006).
[19] Hirayama F, Kasai N, Koyanagi M., “Design of series SQUID array suppressing Josephson oscillation interference between element-SQUIDs,” IEEE Trans. Appl. Supercond. 9(2): 2923-2926 (2002).
[20] Wu W, Lin Z, Ni Z, et al., “Development of series SQUID array with on-chip filter for TES detector,” Chin. Phys. B. 31(2): 028504 (2022).
[21] Drung D, Abmann C, Beyer J, et al., “Highly sensitive and easy-to-use SQUID sensors,” IEEE Trans. Appl. Supercond. 17(2): 699-704 (2007).
[22] Doriese W B, Morgan K M, Bennett D A, et al., “Developments in time-division multiplexing of x-ray transition-edge sensors,” J Low Temp Phys. 184(1): 389-395 (2016).
[23] Welty R P, Martinis J M., “A series array of DC SQUIDs,” IEEE Trans. Magn. 27(2): 2924-2926 (2002).
[24] Drung D, Cantor R, Peters M, et al., “Low-noise high-speed dc superconducting quantum interference device magnetometer with simplified feedback electronics,” Appl. Phys. Lett. 57(4): 406-408 (1990).
[25] Rudolph M, Nagel J, Meckbach J M, et al., “Direct current superconducting quantum interferometers with asymmetric shunt resistors,” Appl. Phys. Lett. 101(5): 052602 (2012).
[26] Lolli L, Taralli E, Rajteri M, et al., “Characterization of optical fast transition-edge sensors with optimized fiber coupling,” IEEE Trans. Appl. Supercond. 23(3): 2100904-2100904 (2013).